Motor unit mechanisms of speed control in mouse locomotion

Kyle Thomas[1], Rhuna Gibbs[2], Hugo Marques[3], Megan R. Carey[3], Samuel J. Sober[2]

[1]Graduate Program in Biomedical Engineering, Emory University and Georgia Institute of Technology, Atlanta, United States; [2]Department of Biology, Emory University, Atlanta, United States; [3]Champalimaud Neuroscience Programme, Champalimaud Centre for the Unknown, Lisbon, Portugal

Abstract

During locomotion, the coordinated activity of dozens of muscles shapes the kinematic features of each stride, including systematic changes in limb movement across walking speed. Motor units, each of which consists of a single motor neuron and the muscle fibers it innervates, contribute to the total activation of each muscle through their recruitment and firing rate when active. However, it remains unknown how the nervous system controls locomotor speed by changing the firing of individual motor units. To address this, we combined quantitative behavioral analysis of mouse locomotion with single motor unit recordings from the lateral and long heads of the triceps brachii, which drive monoarticular extension of the elbow and biarticular movements of the elbow and shoulder, respectively. In contrast to prior studies employing bulk EMG to examine muscle activity, our recordings revealed the diversity of spike patterning across motor units as well as systematic differences in motor unit activity across muscles and locomotor speeds. First, motor unit activity differed significantly across the lateral and long heads, suggesting differential control of these two closely apposed elbow extensor muscles. Second, we found that individual units were recruited probabilistically during only a subset of strides, showing that bulk EMG signals consistently present in every stride in fact reflect stochastically varying subsets of individual motor units. Finally, although recruitment probability and firing rate both increased at faster walking speeds, increases in recruitment were proportionally larger than rate changes, and recruitment of individual units accompanied changes in limb kinematics. Together, these results reveal how the firing of individual motor units varies systematically across muscles and walking speeds to produce flexible locomotor behavior.

Introduction

Skilled behavior depends on the nervous system's precise control of muscle activity. Motor units, which consist of a single motor neuron and all of the muscle fibers it innervates, generate the forces behind movement through their firing patterns. In locomotion, proper neural coordination of motor units within and across muscles allows for the stereotyped yet rapidly adjustable movement used for each step (Akay et al., 2014; Mayer & Akay, 2018; N. P. Schumann et al., 2006). In principle, the total force output of a muscle is modulated by the number of recruited motor units and the firing rate of active units (Enoka & Duchateau, 2017; Heckman & Enoka, 2012), with each newly-recruited unit increasing total muscle force by activating more muscle fibers. The firing rate and inter-spike-interval (ISI) pattern of recruited units then shape force production in concert with the biomechanics of the musculoskeletal system (Sober et al., 2018; Sponberg et al., 2011). Although studies in primates, cats, and zebrafish have shown that both the number of active motor units and motor unit firing rates increase at faster locomotor speeds (Grimby, 1984; Hoffer et al., 1981, 1987; Marshall et al., 2022; Menelaou & McLean, 2012), the extent to which speed-dependent changes in rate and recruitment vary across muscles and species is unknown.

Mice demonstrate both physiological and biomechanical differences from other vertebrates, potentially leading to unique coordination among their motor units. Compared to cats, for example, mice have highly excitable motor units (Manuel et al., 2019; Manuel & Heckman, 2011) with muscle fibers heavily biased towards fast-twitch fibers (Burkholder et al., 1994; Mathewson et al., 2012), leading to rapid force production. Mice also locomote with greater stride frequency than larger species in order to achieve comparable speeds, requiring faster muscle activation and deactivation (Heglund & Taylor, 1988; Machado et al., 2015). The capability and need for faster force generation during dynamic behavior could implicate motor unit recruitment as a primary mechanism for modulating force output in mice.

To quantify the organization of motor unit firing patterns during locomotion, we recorded mouse motor unit activity from the long head and lateral head of the triceps brachii during treadmill walking at various speeds. Both muscles extend the elbow while the long head also extends, rotates, and abducts the shoulder (Tata Ramalingasetty et al., 2021). Although the triceps are active in every step during quadrupedal locomotion (A. W. English, 1978; Kirk et al., 2024; N. Schumann, 2002), it is unknown how individual motor units are coordinated to generate this rhythmic pattern and whether motor pools from closely apposed muscles would exhibit the same coordination. Using Myomatrix electrodes (Chung et al., 2023) to record populations of individual motor units during locomotion, we found that units were recruited probabilistically across strides. When active, units fired in distinct locomotor phases with systematic differences in spike patterns across the long and lateral heads. At faster walking speeds, motor units increased both their recruitment probabilities and (to a lesser extent) their firing rates. Moreover, motor unit recruitment predicted variations in limb kinematics both within and across locomotor speeds, with recruitment of long head and lateral head units associated with different changes in limb movement. Overall, our results reveal the systematic changes in motor unit firing that regulate locomotor speed.

Results

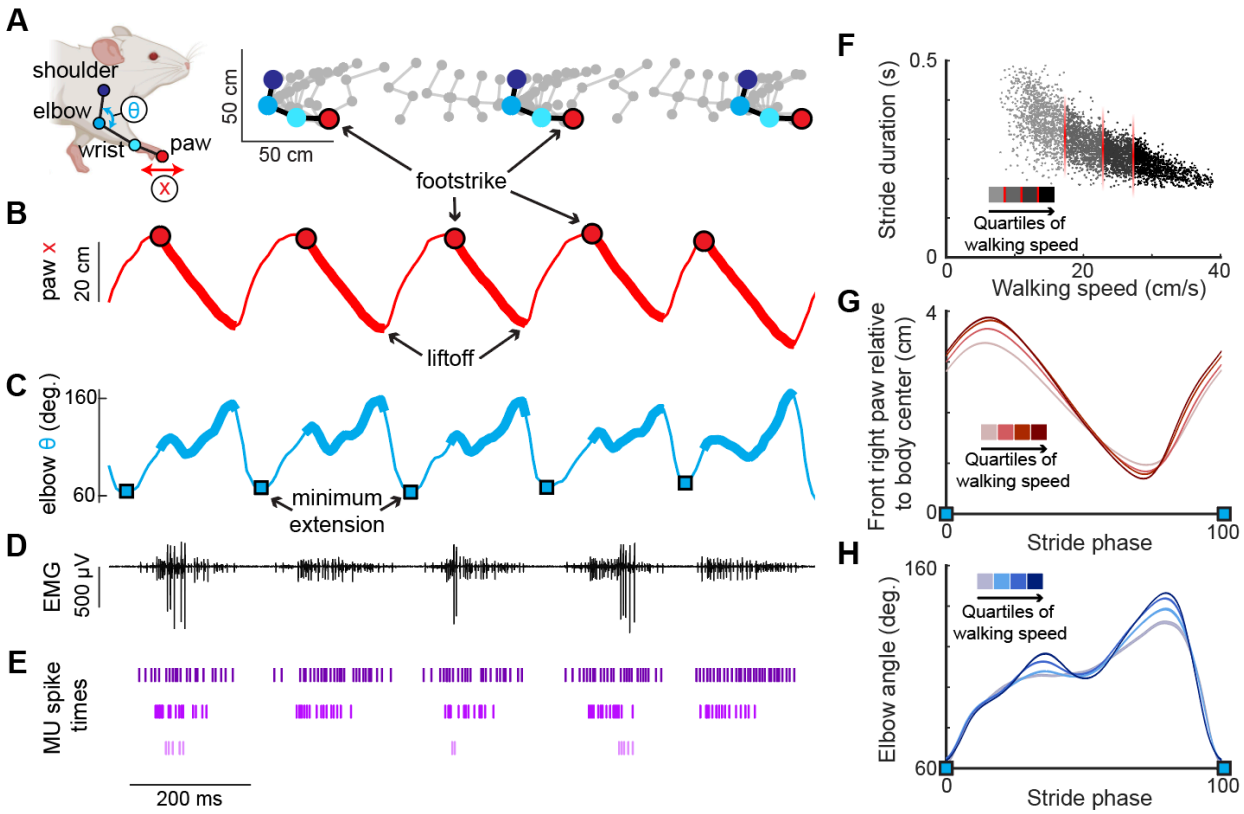

Figure 1. High-resolution muscle recording during mouse locomotion. **(A)** (Left) Anatomical landmarks (shoulder, elbow, wrist, paw) and kinematic features (elbow angle θ, paw position x) tracked via high-resolution video during treadmill walking (Darmohray et al., 2019; Mathis et al., 2018). (Right) Position of anatomical landmarks during two stride cycles with limb position captured every 15 ms. **(B)** Position of the right forepaw (x) relative to body center. Thick lines represent the stance phase when the paw is on the ground. **(C)** Interior elbow angle (θ) during locomotion. Troughs of this measure, denoting minimum extension (blue squares), were used to define the spike window for each stride. **(D)** Representative channel of electromyographic (EMG) activity in the long head of the right triceps used to isolate several motor units during walking. **(E)** Three motor units from the long head identified from the above EMG trace (see Methods). Note that units may only be active in a subset of strides. **(F)** Relationship between stride duration and walking speed for all strides in an example mouse. Each dot represents a stride, with shading indicating the speed quartile within which the stride falls (see Methods). **(G,H)** Right forepaw position x (G) and elbow angle (H) within the walking speed quartiles. Note that both (G) and (H) are normalized to total stride duration beginning and ending with elbow minimum extension (blue squares) and show mean (± SE).

We collected kinematic and high-resolution electromyographic (EMG) data from six mice walking on a transparent treadmill that provided simultaneous lateral and ventral views of the

animal (Darmohray et al., 2019). Using DeepLabCut (Mathis et al., 2018) to track body movements during locomotion (Fig. 1A), we identified the stance phase of the right forelimb, defined as the period between footstrike and liftoff of the right forepaw (Fig. 1B). Additionally, computing the internal angle of the elbow joint revealed that the elbow was minimally extended approximately 50 milliseconds before the footstrike (blue squares, Fig. 1C). Electrode arrays (32-electrode Myomatrix array model RF-4x8-BHS-5) were implanted in the triceps brachii (note that Fig. 1D shows the EMG signal from only one of the 16 bipolar recording channels), and the resulting data were used to identify the spike times of individual motor units (Fig. 1E) as described previously (Chung et al., 2023). To best capture the spike pattern given that some units begin firing prior to footstrike, we defined a stride cycle as the period between minimum elbow angles rather than consecutive footstrikes. Kinematic analysis of locomotor data at different walking speeds revealed systematic variation in the temporal (Fig. 1F) and spatial (Fig. 1G-H) components of limb movement, consistent with prior reports (Akay et al., 2006; Bellardita & Kiehn, 2015; Machado et al., 2015; Mendes et al., 2015).

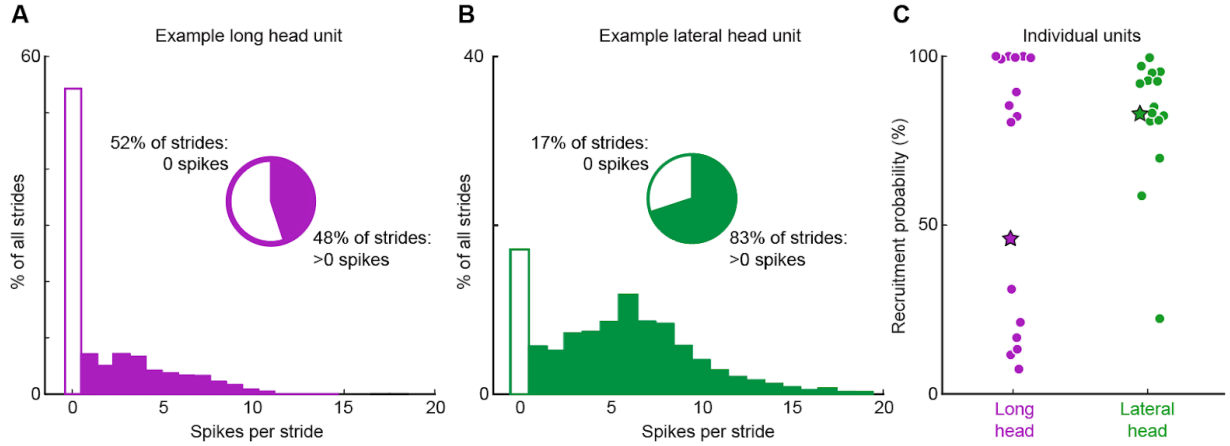

Figure 2. Motor unit spike count distributions. **(A)** Example motor unit from the long head of the triceps muscle fired zero spikes on 52% of strides, but on the other 48% of strides fired 1-14 spikes. **(B)** Example motor unit from the triceps lateral head fired zero spikes in 17% of strides but 1-19 spikes on the other 83% of strides. **(C)** Percentage of strides with at least one spike (probability of recruitment) for all recorded motor units in the long (purple) and lateral (green) heads of the triceps. Each dot reflects an individual motor unit and starred points refer to the examples in (A) and (B).

Motor units are probabilistically recruited across strides

Despite the triceps muscles as a whole being reliably activated on every step (A. W. English, 1978; Kirk et al., 2024; N. Schumann, 2002), the majority of individual motor units in both the long head and lateral head were active only in a subset of strides during locomotion. Motor units in both muscles exhibited this pattern of probabilistic recruitment but with differing distributions of firing properties across the long and lateral heads (Fig. 2). For each motor unit, we measured

the probability of a unit being recruited as the percentage of strides with at least one spike. Units often displayed no recruitment in a greater proportion of strides than for any particular spike count when recruited (Fig. 2A,B), and units that were less likely to be recruited also had lower average spike counts (Supplemental Fig. 1). A subpopulation of units, primarily in the long head, were recruited in under 50% of the total strides and with lower spike counts (Fig. 2C). We did not identify a prominent second group of units with low recruitment probability within the lateral head, suggesting that these two triceps muscles might contain functionally different subpopulations of motor units (see Discussion).

Motor unit firing patterns in the long and lateral heads of the triceps

Motor units within each muscle fired at distinct phases of the stride cycle. Units in the long head typically became active near the time of footstrike, with approximately half of the units reliably recruited prior to footstrike (Fig 3A,B). In contrast, units in the lateral head began spiking after the long head was already active and remained active until just prior to liftoff (Fig. 3B,C). Furthermore, units in the long head reached their stride-dependent peak rates before the lateral head ($p<0.01$, two-sample k-s test). These findings demonstrate that despite the overlapping biomechanical functions of the long and lateral heads of the triceps, the nervous system creates a consistent, approximately 100 ms delay (Fig. 3C) between the activation of the two muscles' motor neuron pools. This timing difference suggests distinct patterns of synaptic input onto motor neurons innervating the lateral and long heads. In contrast to the timing differences described above, motor units in the lateral and long heads displayed similar burst durations (Fig. 3B) and peak firing rates (Fig. 3D).

The evolution of spike patterns within each stride differed between motor unit populations in the long and lateral heads. In both muscles, motor units with longer burst durations reached higher peak firing rates (Fig. 4A). However, the slope of this relationship was significantly higher ($p<0.01$) for lateral head units. We also observed muscle-dependent differences in motor unit patterning when examining the inter-spike intervals (ISIs) between the first three spikes in each stride cycle. Motor units in both muscles began firing with ISIs typically below 12 ms (Fig 4B). Furthermore, the second ISI was generally shorter, indicating that firing rate increased throughout the first three spikes fired in the stride cycle. However, the population of motor units in the long head had a larger magnitude in the ratio ISI_1/ISI_2 (Fig. 4B, $p<0.01$, two-sample k-s test). Together with the differences in burst timing shown in Figure 3B, these results again suggest that the motor pools for the lateral and long heads of the triceps receive distinct patterns of synaptic input, although differences in the intrinsic physiological properties of motor neurons innervating the two muscles might also play an important role.

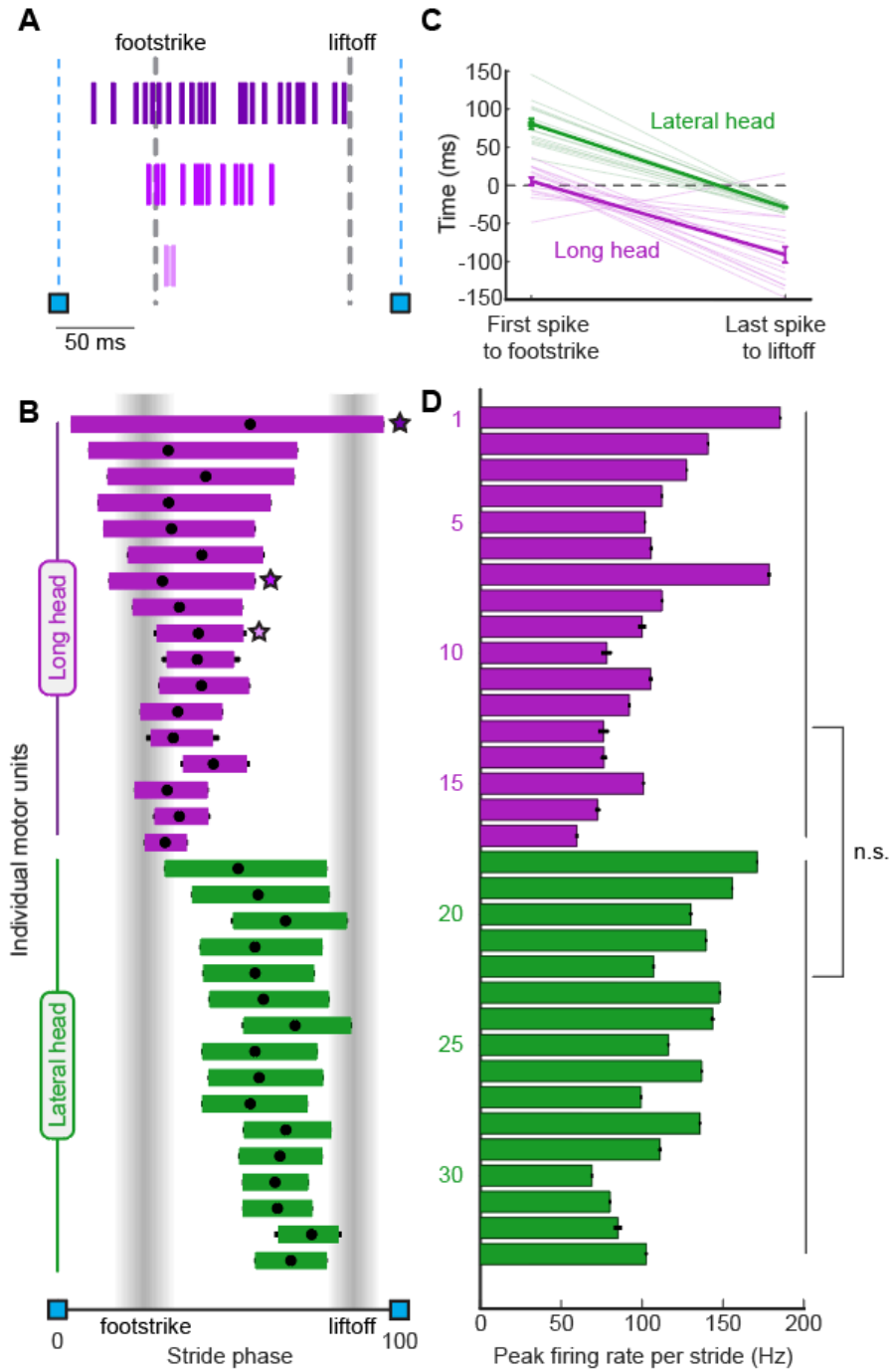

Figure 3. Motor unit firing patterns within and across muscles. **(A)** Example stride with three units from the long head. **(B)** Mean phase (± SE) of motor unit burst duration across all strides. Black dot within each bar shows the mean phase of the unit's peak firing rate. Starred points refer to the examples in A. **(C)** Left: Mean time (± SE) between the first spike of a unit's spike train and the right forepaw footstrike. Positive values denote the spike happening after the footstrike. Right: Mean time (± SE) between the last spike of a unit and the liftoff. Light traces denote values for individual motor units while the heavy trace shows the mean and standard error across all units within a muscle. **(D)** Mean peak firing rate (± SE) of each unit. Note that these measurements only include strides in which the given unit was recruited.

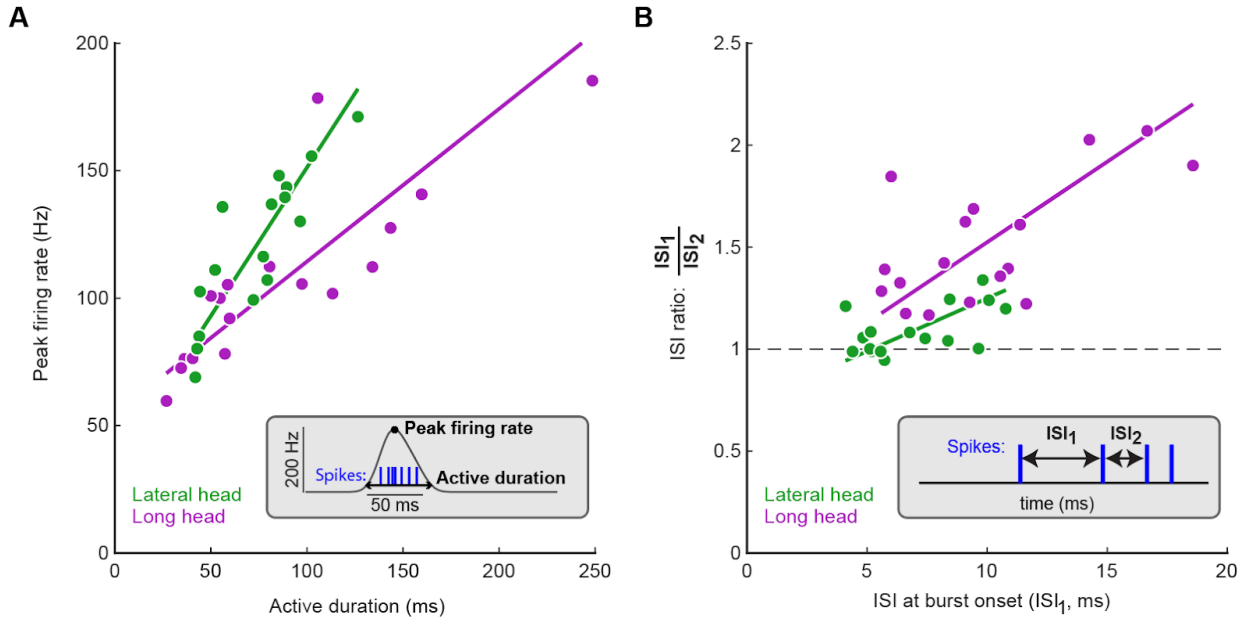

Figure 4. Motor unit spike patterns evolve differently in the long and lateral heads. **(A)** Relationships between active duration and peak firing rate across motor pools. Linear (type 2) regression analysis for the lateral head (R^2 = 0.74, p<0.0001) and long head (R^2 = 0.70, p<0.0001); regression slopes were significantly different between the lateral and long heads (p<0.01). **(B)** Motor unit inter-spike intervals (ISIs) across the first three spikes in motor unit bursts. Each data point shows the mean of the first ISI and the ratio between the first and second ISIs for a single unit. Note that by definition only strides with at least three spikes could be used for the analysis shown in panel (B). Linear (type 2) regression analysis for the lateral head (R^2 = 0.30, p<0.05) and long head (R^2 = 0.42, p<0.05); regression slopes were not significantly different between data from the lateral and long heads.

Motor unit mechanisms of speed control

Adjusting walking speed requires changes in the firing patterns of individual motor units, which could include speed-dependent changes in units' probability of recruitment and/or changes in firing rate. To investigate the changes in motor unit firing underlying locomotor speed control, we quantified how both recruitment probability and firing rate change across the four quartiles of locomotor speed shown in Figure 1F-H. Motor units from the long and lateral heads of the triceps (Fig. 5A,B, purple and green traces, respectively) displayed significant increases in recruitment probability as locomotor speeds increased. Figure 5C shows each motor unit's difference in recruitment probability between the slowest and fastest locomotor speed quartiles. This increase was statistically significant in 29/33 motor units in our study (p<0.05, bootstrap confidence interval) when considered individually, and was also significant when the probabilities of all motor units were analyzed as a group (p<0.01, Wilcoxon signed-rank test). Robust increases in recruitment probability across the four speed quartiles were therefore the norm in our dataset.

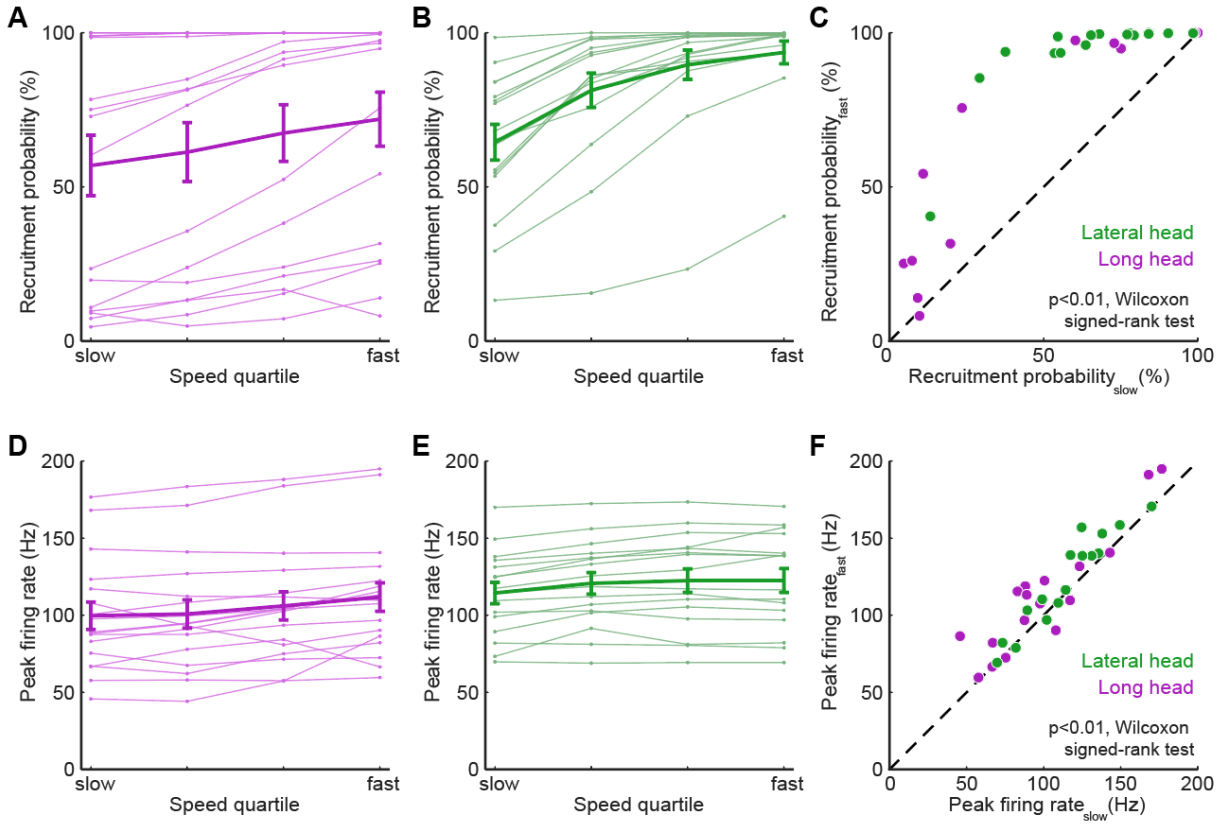

Figure 5. Motor units alter firing rate and recruitment across walking speeds. **(A)** Light traces show median of recruitment probability for individual long head motor units while the heavy trace shows mean (± SE) across all long head motor units. **(B)** Recruitment probability for lateral head motor units, same plotting conventions as in (A). **(C)** Difference in recruitment probabilities between slowest and fastest speed quartiles for all motor units. **(D)** Light traces show median of peak firing rate for individual long head motor units while the heavy trace shows mean (± SE) across all long head motor units. **(E)** Peak firing rates for lateral head motor units, same plotting conventions as in (D). **(F)** Difference in peak firing rates between slowest and fastest speed quartiles for all motor units. Across all motor units, both recruitment probabilities (C) and firing rates (F) were significantly higher at the fastest quartile than at the slowest quartile ($p<0.01$, Wilcoxon signed-rank tests). Speed-dependent changes in recruitment vs speed-dependent changes in firing rate for individual motor units are shown in **Supplemental Figure 2**.

Quantitative analysis of motor unit activity also revealed significant speed-dependent changes in firing rate, although these were proportionally smaller than the increases in recruitment probability. Motor units in both the long and lateral heads of the triceps (Fig. 5D,E, purple and green traces, respectively) often had either marginal increases or no difference in peak firing rate at faster speeds. Across all motor units in our dataset in the slowest and fastest speed quartiles (Fig. 5F), we observed significant increases in peak firing rate in 20/33 individual motor units in our study ($p<0.05$, bootstrap confidence interval), and also a significant speed-dependent increase in peak rate when considering all motor units together ($p<0.01$, Wilcoxon signed-rank test). Speed-dependent increases in peak firing rate were therefore also

present in our dataset, although in a smaller fraction of motor units than changes in recruitment probability. Furthermore, the average magnitude of speed-dependent increases was smaller for spike rates (mean $rate_{fast}/rate_{slow}$ of 111% across all motor units) than for recruitment probabilities (mean $p(recruitment)_{fast}/p(recruitment)_{slow}$ of 179% across all motor units). These findings suggest that while both recruitment and peak rate change across speed quartiles, increased recruitment probability likely plays a larger role in driving changes in locomotor speed.

Kinematic contributions of motor unit recruitment

We next examined whether the probabilistic recruitment of individual motor units in the triceps – an elbow extensor muscle – predicted stride-by-stride variations in elbow angle kinematics. To do so, we compared elbow extension ($\Delta\theta$; Fig. 6A) on strides in which each individual motor unit did or did not fire at least one spike. When kinematic data are combined across all speed quartiles (Fig. 6B), we found that recruitment of lateral head motor units (green symbols) is associated with greater elbow extension, whereas recruitment of long head units (purple symbols) predicts smaller extensions ($p<0.001$, Wilcoxon signed-rank tests). These correlations might reflect both an influence of motor unit recruitment on limb kinematics as well as different biomechanical roles for the long and lateral heads.

Since both limb kinematics (Fig. 1G,H) and recruitment probability (Fig. 5) are significantly correlated with locomotor speed, the observed correlation between unit recruitment and elbow extension across all speeds (Fig. 6B) does not necessarily reveal the direct influence of unit firing on limb kinematics. We therefore controlled for speed by repeating the analysis shown in Figure 6B for strides within each speed quartile. Strikingly, the correlations between motor unit recruitment and elbow angle persisted in this alternative analysis (Fig. 6C; $p<0.001$, Wilcoxon signed-rank tests), suggesting that the recruitment of individual motor units in the lateral and long heads might have significant (and opposite) effects on elbow angle in strides of similar speed (see Discussion).

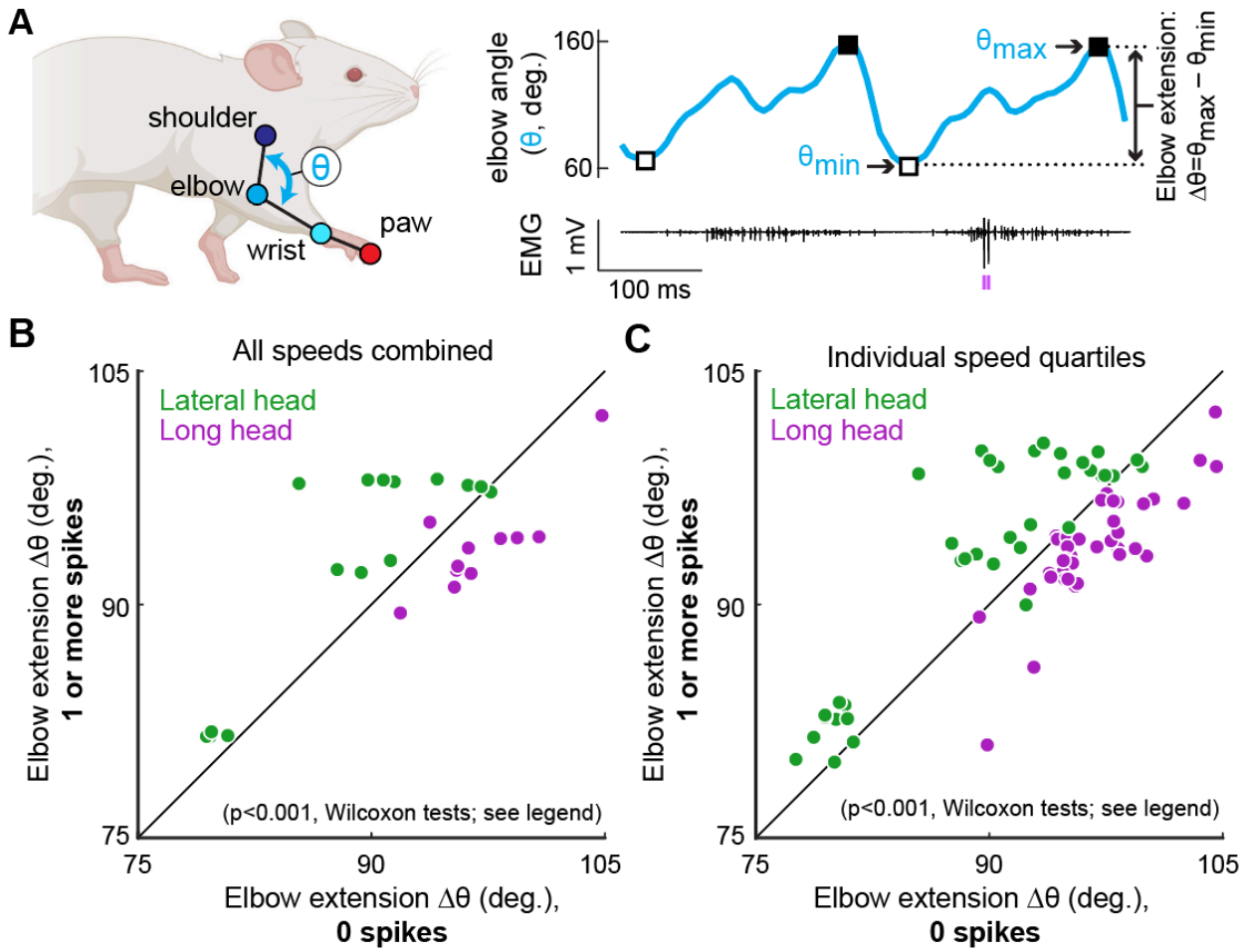

Figure 6: Motor unit recruitment predicts muscle-specific kinematic differences. **(A)** We defined elbow extension ($\Delta\theta$) as the total extension of the elbow over one stride cycle ($\Delta\theta = \theta_{max} - \theta_{min}$) on strides in which each motor unit did or did not fire at least one spike (purple tick marks below EMG trace). **(B)** Each point represents the mean elbow extension observed on strides in which a single motor unit from the lateral (green) or long (purple) head of the triceps fires zero spikes (horizontal axis) vs. when the motor unit fires at least one spike (vertical axis). Stride cycles during which lateral head motor units were recruited (fired at least one spike) exhibited significantly larger elbow extensions than those without spiking ($p<0.001$, Wilcoxon signed-rank tests), and strides during which long head units were recruited showed significantly smaller elbow extensions than those without spiking ($p<0.001$, Wilcoxon signed-rank test). Note that in this panel, data for each motor unit were combined across all locomotor speeds. Panel **(C)** shows the same analysis as in (B), except that each motor unit contributes up to four data points, one for each of the four locomotor speed quartiles in which sufficient data were available (at least 30 strides existed in both the spiking and non-spiking conditions within a given quartile). This analysis yielded the same result as the one shown in panel (B), with the presence of a spike in the lateral head (green) associated with greater elbow extension and the presence of a spike in the long head (purple) associated with lesser elbow extension ($p<0.001$, Wilcoxon signed-rank tests). Note that most of the muscle-specific differences shown in (C) were also present when each of the four quartiles were examined individually for each muscle (see **Supplemental Figure 3 – supplement to figure 6**).

Discussion

Our data reveal the diversity of motor unit firing patterns in mouse triceps brachii muscles during walking. Motor units were probabilistically recruited on a stride-by-stride basis with peak firing rates between 60-185 Hz when active. Motor units in the long head were recruited before the lateral head and spiking patterns evolved within each stride differently across the two muscles. Motor units in both muscles demonstrated increases in their recruitment probability and firing rate at faster walking speeds. Furthermore, motor unit recruitment was also correlated with differences in limb kinematics for strides of similar speed. As discussed below, firing patterns from motor units in the long and lateral heads likely reflect the functional and anatomical role of these two muscles, highlighting the need for high-resolution quantification of motor unit firing patterns during behavior.

Differences in motor unit activity patterns across two elbow extensors

Motor unit spike patterns differed systematically between the long and lateral heads of the triceps brachii. Motor units in the long head were consistently recruited earlier than units in the lateral head (Fig. 3B,3C). This ordering matches past reports in bulk muscle activity in these two muscles across in other quadrupedal species (Carroll & Biewener, 2009; Drew et al., 2008; Livingston & Nichols, 2014; Scholle et al., 2001) and may reflect the biomechanical functions of each muscle. Whereas the lateral head is a monoarticular elbow extensor, the long head is biarticular, both extending the elbow along with extending and rotating the shoulder (Tata Ramalingasetty et al., 2021). Although we did not measure ground reaction forces, prior reports indicate that the vertical ground reaction force on the mouse forepaw reaches two peaks during locomotion (Schmitt et al., 2010). The first peak, which happens soon after the footstrike, has a lower magnitude than the second peak, which occurs closer to liftoff (Clarke et al., 2001; Schmitt et al., 2010). Studies in both rats (Sarver et al., 2010) and cats (Corbee et al., 2014) have demonstrated that horizontal ground reaction forces in both the medio-lateral and cranio-caudal directions are also greatest soon after footstrike, with more force variability than the vertical reaction force. Since units in the long head are most active following footstrike, this suggests that activity in the long head might be related to stabilizing the limb within each step. Our finding that recruitment of long head motor units (purple symbols, Fig. 6) accompanied smaller elbow extensions might therefore reflect a more complex biomechanical role for the long head. This interpretation is consistent with past findings that biarticular muscles are power distributors, stabilizing the joint across multiple dimensions, while monoarticular muscles are power generators (Ryan & Gregor, 1992; Van Ingen Schenau et al., 1992, 1994). Conversely, the observed timing of lateral head motor unit activity just prior to liftoff (Fig. 3B) might therefore reflect the lateral head's role of providing propulsion prior to swing, consistent with our finding that recruitment of motor units in the lateral head is correlated to larger elbow extension (Fig. 6).

Motor units in the lateral and long heads also differed with respect to their recruitment probabilities, with a substantial population of units in the long head (but not the lateral head) with probability of recruitment less than 50% (Figure 2C). This difference may reflect different functions of muscle fibers in different subcompartments of biarticular muscles. Prior work has established that different regions within a biarticular muscle can have different contributions

across the two joints (Chanaud et al., 1991; A. W. M. English & Weeks, 1987; Watanabe et al., 2021). For example, different regions of the cat biceps femoris are out of phase with each other during walking, with the anterior compartment active during stance as a hip extensor and the posterior compartment active during swing as a knee flexor (Chanaud et al., 1991; A. W. M. English & Weeks, 1987). Additionally, the posterior compartment was only active at faster speeds. In our mouse data, functional compartments within the biarticular long head may thus explain the differently recruited populations for motor units (Fig. 2C). However, to our knowledge, no studies have investigated anatomical or functional subdivisions across subregions of the triceps long head in the mouse. Nevertheless, the group of less-frequently recruited units might contribute more to forelimb joint stability, which is presumably more variable, whereas the other long head motor units might be recruited in a greater fraction of strides to support the weight of the body. Further examination of the anatomical microstructure of the long head, including precise characterization of the attachment points to the bone (DeWolf et al., 2024; Gilmer et al., 2024), are necessary to answer these questions.

The varied composition of fiber types in the long and lateral heads may also explain the different firing patterns across muscles. Although both muscles are heavily biased towards the fastest myosin type (type 2B), the long head has a broader composition, including a small percentage of slower isoforms as well (type 1 and 2A) (Mathewson et al., 2012). Type 2B isoforms are related to fast-twitch, fatigable units (FF) while type 1 compose slow-twitch units (S) (Bączyk et al., 2022; Schiaffino & Reggiani, 2011). While we were unable to directly quantify the unit type, the majority of units observed, particularly within the lateral head, are likely FF units given the mouse anatomy. Thus, the probabilistic recruitment may be related to units' susceptibility to fatigue throughout approximately 30 minutes of locomotion (Martínez-Silva et al., 2018). Experimenters randomly changed between slow and fast treadmill speeds every trial, each of which lasted a minute, but fatigue may have still set in within a trial or over the experiment's duration. Motor units that were recruited in nearly every stride with 10 or more spikes per stride (supp. Fig 1) could result from units with slower isoforms given their resistance to fatigue. The most prominent example of this came from the single unit in the long head that fired for over 90% of the stride phase in every stride. Still, given the wide range of firing patterns and tendency for units to be recruited more reliably at fast speeds (Fig. 5), our estimation of unit type differences within each muscle only begins to explain the nuanced details of motor unit function during locomotion.

Firing rates in mouse locomotion compared to other species

The range of firing rates we observed are faster than typically observed across larger species, likely reflecting the unique physiology of mouse motor neurons. Motor units in the lateral and long heads of the triceps exhibited a large and overlapping range of peak firing rates ranging from 50-175 Hz (Fig. 3D), in agreement with prior reports of motor unit firing rates from mouse forelimb (Kirk et al., 2024) and hindlimb (Hadzipasic et al., 2016) during locomotion. In rat hindlimb muscles during walking, motor units had mean instantaneous firing rates between 45-109 Hz (Gorassini et al., 2000). Notably, motor units across the tibialis anterior, medial gastrocnemius and lateral gastrocnemius also typically fired rapidly at the beginning of each stride, often with ISIs around 5 ms before settling into a slower, more consistent rate. Since several units in this study only fired once in a large proportion of strides when active,

observations of ISIs, while helpful for directly calculating instantaneous firing rates, might also be limiting for an overall interpretation of firing patterns. Still, while we also found short ISIs at the beginning of the stride, these did not seem to precede a consistent rate drop. During cat locomotion, motor units recorded from the toe and hindlimb had firing rates between 15-50 Hz (Hoffer et al., 1987; Zajac & Young, 1980). Human motor units in the short extensors of the toe fire at even lower rates (10-25 Hz) during walking (Grimby, 1984). Compared to these larger species, mice likely reach higher rates through the physiological properties of their motor neurons such as afterhyperpolarization (AHP), which influences how rapidly a neuron returns to baseline voltage after firing a spike. Although AHP durations vary across unit types, AHP durations in mice are approximately two and three times shorter than those in cats and humans respectively (Manuel et al., 2009, 2019; Meehan et al., 2010). Additionally, persistent inward currents (PICs), which amplify excitatory synaptic inputs (Binder et al., 2020; Heckman et al., 2005), might lead to disproportionately large gain in mouse motor neurons compared to other species (Huh et al., 2017; Manuel et al., 2019). Consequently, even mice performing quiet standing have motor unit firing rates reaching up to 68 Hz (Ritter et al., 2014). Our findings (Fig. 4) highlight that even with the relatively high firing rates observed in mice, there are still significant changes in firing rate across the spikes within bursts (Fig. 4B) and across locomotor speeds (Fig. 5F).

Walking speed modulation of firing rate and recruitment

To investigate the neuromuscular control of locomotor speed, we quantified speed-dependent changes in both motor unit recruitment and firing rate. We found that the majority of units were recruited more often and with larger firing rates at faster speeds (Fig. 5, Supplemental Fig 2). Importantly, our work only examines a subset of the movement speeds and gait patterns that mice produce. It therefore remains to be determined how rate and recruitment are reshaped as mice increase their speed up to 100 cm/s and alter coordination patterns across their limbs (trotting, bounding, etc.) (Herbin et al., 2006, 2007; Bellardita & Kiehn, 2015; Gonçalves et al., 2022). Since a majority of observed motor units, particularly in the lateral head, were already reliably recruited at the fastest speed quartile (roughly 30-40 cm/s), further speed increases might rely on either more firing rate modulation from these active units or from recruitment of more of the motor pool. Moreover, adjustments to kinematic and kinetic strategy across speeds could result from more global changes in motor unit coordination. For example, studies in drosophila (Azevedo et al., 2020) and zebrafish (Kishore et al., 2014) have demonstrated preferential recruitment of faster motor unit subtypes during rapid movements. Future studies in mice can therefore examine faster gaits to compare how different species achieve their most rapid forms of locomotion.

Considering the force production of motor units is essential to connect our observations of firing patterns to behavioral outputs. In anesthetized mice, intracellular current injections into individual motor neurons revealed that fast motor units from the triceps surae (gastrocnemius and soleus muscles of the hindlimb) reached near tetanic force at firing rates between 60-80 Hz while slow motor units reached near tetanic forces between 30-40 Hz (Manuel & Heckman, 2011). Furthermore, motor units rapidly reached these rates once active. Despite being recorded from different muscles than the ones we examined, these earlier results are relevant to our findings given that the long and lateral heads of the triceps brachii are (similarly to the

gastrocnemius) biased towards fast-twitch muscle fibers (Augusto et al., 2004; Burkholder et al., 1994). Given that motor units recorded in our study had firing rates at or above the aforementioned rates immediately upon recruitment within a stride (Fig. 4B), it could be that each of the units identified in this study generated near-maximal force whenever active. If units are recruited with near maximal force even at slow walking speeds, generating the additional forces needed for fast walking likely comes from recruitment of additional units. Future studies might answer this question by quantifying the force-production properties of triceps motor units during the rapid changes in the muscle length and shortening velocity that take place during locomotion (Edman, 1979; Gittings et al., 2012; Ting & Chiel, 2017).

Future studies might also use perturbations of muscle activity to dissociate the causal properties of each motor unit's activity from the complex correlation structure of locomotion. Despite the strong correlations observed between motor unit recruitment and limb kinematics (Fig. 6, Supplemental Fig. 3), these results might reflect covariations of both factors with locomotor speed rather than the causal properties of the recorded motor unit. This caveat also exists in the correlations identified within individual speed quartiles (Fig. 6C). To isolate the effects of motor unit recruitment, future studies might therefore use a perturbative approach of electrically or optically stimulating a single muscle and measuring the resulting changes in kinematics (Kim et al., 2024; Lu et al., 2024; Srivastava et al., 2015, 2017). The short-latency effects of patterned motor unit stimulation (Srivastava et al., 2017) could then reveal the sensitivity of behavior to changes in muscle spiking or the extent to which the same behaviors can be performed with many different motor commands.

Methods

Surgical implantation

All procedures described below were approved by the Emory University Institutional Animal Care and Use Committee at Emory University (IACUC protocol #201700359). Mice were anesthetized with isoflurane to implant the Myomatrix arrays. Incisions were made in the skin both on the skull and above the target muscle. Forceps were used to pull the Myomatrix array through these holes so that the body of the array was entirely subcutaneous, with the Omnetics connector sitting on the skull and the array threads near the muscles. The surface of the skull was scored, and dental cement (Metabond Quick Adhesive Cement) was applied generously to fix the Omnetics connector in place and seal the opening. The threads were then sutured (8-0 non-absorbable suture from AROSurgical) into the target muscles. Using the four threads on the customizable Myomatrix array (RF-4x8-BHS-5), we implanted a combination of muscles in each mouse, sometimes using multiple threads within the same muscle. Threads were implanted in the triceps brachii long head and/or the triceps brachii lateral head and confirmed through expert visual inspection. We did not implant in the third (medial) head of the triceps given that it would have required an additional incision, posing more risk of surgical complications. Some mice also had threads simultaneously implanted in their ipsilateral or contralateral biceps brachii although no data from the biceps is presented in this study. Lastly, 6-0 suture was used to close

the incision. Surgeries typically took under three hours and animals were mobile shortly after removal from isoflurane.

Behavioral methods and data collection

The treadmill used in this task had a transparent belt and base as described previously (Darmohray et al., 2019; Machado et al., 2015). A 45° angled mirror below the base allowed monitoring of side and bottom views from a single camera (FLIR Grasshopper High Performance USB 3.0 Monochrome Camera) at 330 frames per second. Separate motors controlled the left and right belts, but both were run at the same speed for every experiment. The treadmill, placed within a behavior box, was dark, with the only source of light coming from infrared light.

Experiments were conducted the day following the implant surgery up to five days post-surgery. Data presented in this study came from the first day of recording, in which signal quality tended to be greatest (Chung et al., 2023). In each experimental session, mice were first briefly placed under anesthesia using isoflurane to attach a lightweight (1g) digitizing headstage (Intan RHD 16-Channel Bipolar-Input Recording Headstage) to the Omnetics connector on their skulls. Each recording session lasted approximately 45 minutes in total, and we waited at least 10 minutes after removal from isoflurane to ensure all animals were fully awake before recording began.

For five of six mice, we attempted to record 31 trials - each trial consisted of a single minute continuous running on the treadmill. The first three trials were at 10 cm/s, while the following trials were arranged in seven blocks of four trials each. Each block contained a trial at 12.5 cm/s, 17.5 cm/s, 22.5 cm/s, and 27.5 cm/s in a random order presented identically across mice. This pseudo-random order of speeds as opposed to a strict ramping order ensured that we collected data across the full range while reducing potential effects of fatigue. For mice that became uncooperative before completing all trials, we ended the experiment early. Of these five mice, three mice completed all 31 trials, one completed 30, and the last completed 23 trials. For the sixth mouse, we again began with three trials at 10 cm/s, but only increased the speed in 2.5 cm/s increments for either two or three trials each up to a total of 14 trials. Mice were trained on their given running paradigm and habituated to the treadmill setup twice prior to surgery. Each trial was initiated using custom Bonsai software (Lopes et al., 2015) and Arduino components to synchronize neural recordings with the camera and motor output.

We used DeepLabCut (Mathis et al., 2018) to track body parts of the mouse during locomotion (Fig. 1a). We excluded points tracked with less than 90% confidence from DLC and interpolated those points from adjacent high-confidence points. The right elbow angle was estimated using markers from the shoulder, elbow, and wrist. We defined strides using the trough-to-trough minimums of the elbow angle, which occurred approximately 50-100 ms before the footstrike of the right paw. Each stride was also required to contain footstrike and liftoff of the right forepaw during forward movement. From here, we excluded strides with stride durations, stance durations, swing durations, body velocities, or body accelerations outside their respective 95% confidence interval. As a result, we kept about 80% of strides for each animal. Five of six mice

had between 2600-3600 total strides, and the remaining mouse, which was run at the slower speed range, had just over 1000 strides included in analyses.

Electromyography (EMG)

Bipolar signals from adjacent contact pairs on the Myomatrix array were extracted at 30 kHz (Intan RHD Recording Controller) and bandpassed between 300-7500 Hz. Using up to 16 channels of high-resolution EMG from the Myomatrix arrays, motor units were identified using Kilosort 2.5, an open-source multi-channel spike sorting algorithm (Pachitariu et al., 2016). We slightly adjusted the algorithm to better fit the assumptions behind motor unit activity, including the removal of spatial decay across channels. A full description of adjustments has been previously reported (Chung et al., 2023). A total of 33 units were identified and manually verified across all animals. Sorting was high enough quality that no strides were excluded due to inseparable unit activity.

Data analysis

Continuous firing rates were calculated by convolving raw spike times of a motor unit with a Gaussian kernel with σ = 10 ms. This continuous result was phase-normalized across strides before calculating the mean continuous rate to identify relevant patterns such as the unit's active duration or peak firing rate. Active duration was measured between the first and last time within a stride that the smoothed curve reached the half-height from a single spike. Overall, this method allowed for quantification of firing rates even when only a single spike was present for a stride.

To quantify recruitment probability and firing rate when active, we modeled the parameters together by fitting a Poisson distribution to the peak firing rate, scaled by the recruitment probability, across all strides with spiking activity. Strides without spiking activity had the above added to the probability of no recruitment. Thus, an inactive unit on a given stride may be the result of either non-recruitment or recruitment with a stochastically zero firing rate. Model estimates had high agreement to empirical observations and were bootstrapped to further calculate 95% confidence intervals. To compare results across speeds, model parameters were fit within each single speed quartile. The 95% confidence interval was again calculated for the differences in model fits across speeds. Parameters were statistically significant if this 95% confidence interval did not include 0.

References

Akay, T., Acharya, H. J., Fouad, K., & Pearson, K. G. (2006). Behavioral and Electromyographic Characterization of Mice Lacking EphA4 Receptors. *Journal of Neurophysiology*, *96*(2), 642–651. https://doi.org/10.1152/jn.00174.2006

Akay, T., Tourtellotte, W. G., Arber, S., & Jessell, T. M. (2014). Degradation of mouse locomotor pattern in the absence of proprioceptive sensory feedback. *Proceedings of the National Academy of Sciences of the United States of America*, *111*(47), 16877–16882. https://doi.org/10.1073/pnas.1419045111

Augusto, V., Padovani, C. R., & Campos, G. E. R. (2004). Skeletal muscule fiber types in C57BL6J mice. *Braz. j. Morphol. Sci*, 89–94.

Azevedo, A. W., Dickinson, E. S., Gurung, P., Venkatasubramanian, L., Mann, R. S., & Tuthill, J. C. (2020). A size principle for recruitment of Drosophila leg motor neurons. *eLife*, *9*, e56754. https://doi.org/10.7554/eLife.56754

Bączyk, M., Manuel, M., Roselli, F., & Zytnicki, D. (2022). Diversity of Mammalian Motoneurons and Motor Units. In M. J. O'Donovan & M. Falgairolle (Eds.), *Vertebrate Motoneurons* (Vol. 28, pp. 131–150). Springer International Publishing. https://doi.org/10.1007/978-3-031-07167-6_6

Bellardita, C., & Kiehn, O. (2015). Phenotypic Characterization of Speed-Associated Gait Changes in Mice Reveals Modular Organization of Locomotor Networks. *Current Biology*, *25*(11), 1426–1436. https://doi.org/10.1016/j.cub.2015.04.005

Binder, M. D., Powers, R. K., & Heckman, C. J. (2020). Nonlinear Input-Output Functions of Motoneurons. *Physiology*, *35*(1), 31–39. https://doi.org/10.1152/physiol.00026.2019

Burkholder, T. J., Fingado, B., Baron, S., & Lieber, R. L. (1994). Relationship between muscle fiber types and sizes and muscle architectural properties in the mouse hindlimb. *Journal of Morphology*, *221*(2), 177–190. https://doi.org/10.1002/jmor.1052210207

Carroll, A. M., & Biewener, A. A. (2009). Mono- *versus* biarticular muscle function in relation to speed and gait changes: *In vivo* analysis of the goat triceps brachii. *Journal of Experimental Biology*, *212*(20), 3349–3360. https://doi.org/10.1242/jeb.033639

Chanaud, C. M., Pratt, C. A., & Loeb, G. E. (1991). Functionally complex muscles of the cat hindlimb: V. The roles of histochemical fiber-type regionalization and mechanical heterogeneity in differential muscle activation. *Experimental Brain Research*, *85*(2), 300–313. https://doi.org/10.1007/BF00229408

Chung, B., Zia, M., Thomas, K. A., Michaels, J. A., Jacob, A., Pack, A., Williams, M. J., Nagapudi, K., Teng, L. H., Arrambide, E., Ouellette, L., Oey, N., Gibbs, R., Anschutz, P., Lu, J., Wu, Y., Kashefi, M., Oya, T., Kersten, R., … Sober, S. J. (2023). Myomatrix arrays for high-definition muscle recording. *eLife*, *12*, RP88551. https://doi.org/10.7554/eLife.88551

Clarke, K. A., Smart, L., & Still, J. (2001). Ground reaction force and spatiotemporal measurements of the gait of the mouse. *Behavior Research Methods, Instruments, & Computers*, *33*(3), 422–426. https://doi.org/10.3758/BF03195396

Corbee, R. J., Maas, H., Doornenbal, A., & Hazewinkel, H. A. W. (2014). Forelimb and hindlimb ground reaction forces of walking cats: Assessment and comparison with walking dogs. *The Veterinary Journal*, *202*(1), 116–127. https://doi.org/10.1016/j.tvjl.2014.07.001

Darmohray, D. M., Jacobs, J. R., Marques, H. G., & Carey, M. R. (2019). Spatial and Temporal Locomotor Learning in Mouse Article Spatial and Temporal Locomotor Learning in Mouse Cerebellum. *Neuron*, *102*(1), 217–231. https://doi.org/10.1016/j.neuron.2019.01.038

DeWolf, T., Schneider, S., Soubiran, P., Roggenbach, A., & Mathis, M. (2024). *Neuro-musculoskeletal modeling reveals muscle-level neural dynamics of adaptive learning in sensorimotor cortex*. https://doi.org/10.1101/2024.09.11.612513

Drew, T., Kalaska, J., & Krouchev, N. (2008). Muscle synergies during locomotion in the cat: A model for motor cortex control. *The Journal of Physiology*, *586*(5), 1239–1245. https://doi.org/10.1113/jphysiol.2007.146605

Edman, K. A. (1979). The velocity of unloaded shortening and its relation to sarcomere length and isometric force in vertebrate muscle fibres. *The Journal of Physiology*, *291*(1), 143–159. https://doi.org/10.1113/jphysiol.1979.sp012804

English, A. W. (1978). AN ELECTROMYOGRAPHIC ANALYSIS OF FORELIMB MUSCLES DURING OVERGROUND STEPPING IN THE CAT. In *J. exp. Biol* (Vol. 76).

English, A. W. M., & Weeks, O. I. (1987). An anatomical and functional analysis of cat biceps femoris and semitendinosus muscles. *Journal of Morphology*, *191*(2), 161–175. https://doi.org/10.1002/jmor.1051910207

Enoka, R. M., & Duchateau, J. (2017). Rate coding and the control of muscle force. *Cold Spring Harbor Perspectives in Medicine*, *7*(10), 1–12. https://doi.org/10.1101/cshperspect.a029702

Gilmer, J. I., Coltman, S. K., Cuenu, G., Hutchinson, J. R., Huber, D., Person, A. L., & Al Borno, M. (2024). *A novel biomechanical model of the mouse forelimb predicts muscle activity in optimal control simulations of reaching movements*. https://doi.org/10.1101/2024.09.05.611289

Gittings, W., Huang, J., & Vandenboom, R. (2012). Tetanic force potentiation of mouse fast muscle is shortening speed dependent. *Journal of Muscle Research and Cell Motility*, *33*(5), 359–368. https://doi.org/10.1007/s10974-012-9325-6

Gonçalves, A. I., Zavatone-Veth, J. A., Carey, M. R., & Clark, D. A. (2022). Parallel locomotor control strategies in mice and flies. *Current Opinion in Neurobiology*, *73*, 102516. https://doi.org/10.1016/j.conb.2022.01.001

Gorassini, M., Eken, T., Bennett, D. J., Kiehn, O., & Hultborn, H. (2000). Activity of Hindlimb Motor Units During Locomotion in the Conscious Rat. *Journal of Neurophysiology*, *83*(4), 2002–2011. https://doi.org/10.1152/jn.2000.83.4.2002

Grimby, L. (1984). Firing properties of single human motor units during locomotion. *The Journal of Physiology*, *346*(1), 195–202. https://doi.org/10.1113/jphysiol.1984.sp015016

Hadzipasic, M., Ni, W., Nagy, M., Steenrod, N., McGinley, M. J., Kaushal, A., Thomas, E., McCormick, D. A., & Horwich, A. L. (2016). Reduced high-frequency motor neuron firing, EMG fractionation, and gait variability in awake walking ALS mice. *Proceedings of the National Academy of Sciences of the United States of America*, *113*(47), E7600–E7609. https://doi.org/10.1073/pnas.1616832113

Heckman, C. J., & Enoka, R. M. (2012). Motor unit. *Comprehensive Physiology*, *2*(4), 2629–2682. https://doi.org/10.1002/cphy.c100087

Heckman, C. J., Gorassini, M. A., & Bennett, D. J. (2005). Persistent inward currents in

motoneuron dendrites: Implications for motor output. *Muscle & Nerve*, *31*(2), 135–156. https://doi.org/10.1002/mus.20261

Heglund, N. C., & Taylor, C. R. (1988). Speed, Stride Frequency and Energy Cost Per Stride: How Do They Change With Body Size and Gait? *Journal of Experimental Biology*, *138*(1), 301–318. https://doi.org/10.1242/jeb.138.1.301

Herbin, M., Gasc, J.-P., & Renous, S. (2006). How does a mouse increase its velocity? A model for investigation in the control of locomotion. *Comptes Rendus Palevol*, *5*(3–4), 531–540. https://doi.org/10.1016/j.crpv.2005.12.012

Herbin, M., Hackert, R., Gasc, J.-P., & Renous, S. (2007). Gait parameters of treadmill versus overground locomotion in mouse. *Behavioural Brain Research*, *181*(2), 173–179. https://doi.org/10.1016/j.bbr.2007.04.001

Hoffer, J. A., O'Donovan, M. J., Pratt, C. A., & Loeb, G. E. (1981). Discharge Patterns of Hindlimb Motoneurons During Normal Cat Locomotion. *Science*, *213*(4506), 466–467. https://doi.org/10.1126/science.7244644

Hoffer, J. A., Sugano, N., Loeb, G. E., Marks, W. B., O'Donovan, M. J., & Pratt, C. A. (1987). Cat hindlimb motoneurons during locomotion. II. Normal activity patterns. *Journal of Neurophysiology*, *57*(2), 530–553. https://doi.org/10.1152/jn.1987.57.2.530

Huh, S., Siripuram, R., Lee, R. H., Turkin, V. V., O'Neill, D., Hamm, T. M., Heckman, C. J., & Manuel, M. (2017). PICs in motoneurons do not scale with the size of the animal: A possible mechanism for faster speed of muscle contraction in smaller species. *Journal of Neurophysiology*, *118*(1), 93–102. https://doi.org/10.1152/jn.00045.2017

Kim, J. J., Wyche, I. S., Olson, W., Lu, J., Bakir, M. S., Sober, S. J., & O'Connor, D. H. (2024). *Myo-optogenetics: Optogenetic stimulation and electrical recording in skeletal muscles*. https://doi.org/10.1101/2024.06.21.600113

Kirk, E. A., Hope, K. T., Sober, S. J., & Sauerbrei, B. A. (2024). An output-null signature of inertial load in motor cortex. *Nature Communications*, *15*(1), 7309. https://doi.org/10.1038/s41467-024-51750-7

Kishore, S., Bagnall, M. W., & McLean, D. L. (2014). Systematic Shifts in the Balance of Excitation and Inhibition Coordinate the Activity of Axial Motor Pools at Different Speeds of Locomotion. *The Journal of Neuroscience*, *34*(42), 14046–14054. https://doi.org/10.1523/JNEUROSCI.0514-14.2014

Livingston, B. P., & Nichols, T. R. (2014). Effects of Reinnervation of the Triceps Brachii on Joint Kinematics and Electromyographic Patterns of the Feline Forelimb during Level and Upslope Walking. *Cells Tissues Organs*, *199*(5–6), 405–422. https://doi.org/10.1159/000371543

Lopes, G., Bonacchi, N., FrazÃ£o, J., Neto, J. P., Atallah, B. V., Soares, S., Moreira, L., Matias, S., Itskov, P. M., Correia, P. A., Medina, R. E., Calcaterra, L., Dreosti, E., Paton, J. J., & Kampff, A. R. (2015). Bonsai: An event-based framework for processing and controlling data streams. *Frontiers in Neuroinformatics*, *9*. https://doi.org/10.3389/fninf.2015.00007

Lu, J., Zia, M., Baig, D. A., Yan, G., Kim, J. J., Nagapudi, K., Anschutz, P., Oh, S., O'Connor, D., Sober, S. J., & Bakir, M. S. (2024). *Opto-Myomatrix: μLED integrated microelectrode arrays for optogenetic activation and electrical recording in muscle tissue*. https://doi.org/10.1101/2024.07.01.601601

Machado, A. S., Darmohray, D. M., Fayad, J., Marques, H. G., & Carey, M. R. (2015). A

quantitative framework for whole-body coordination reveals specific deficits in freely walking ataxic mice. *eLife*, *4*, e07892. https://doi.org/10.7554/eLife.07892

Manuel, M., Chardon, M., Tysseling, V., & Heckman, C. J. (2019). Scaling of motor output, from mouse to humans. *Physiology*, *34*(1), 5–13. https://doi.org/10.1152/physiol.00021.2018

Manuel, M., & Heckman, C. J. (2011). Adult mouse motor units develop almost all of their force in the subprimary range: A new all-or-none strategy for force recruitment? *Journal of Neuroscience*, *31*(42), 15188–15194. https://doi.org/10.1523/JNEUROSCI.2893-11.2011

Manuel, M., Iglesias, C., Donnet, M., Leroy, F., Heckman, C. J., & Zytnicki, D. (2009). Fast Kinetics, High-Frequency Oscillations, and Subprimary Firing Range in Adult Mouse Spinal Motoneurons. *The Journal of Neuroscience*, *29*(36), 11246–11256. https://doi.org/10.1523/JNEUROSCI.3260-09.2009

Marshall, N. J., Glaser, J. I., Trautmann, E. M., Amematsro, E. A., Perkins, S. M., Shadlen, M. N., Abbott, L. F., Cunningham, J. P., & Churchland, M. M. (2022). Flexible neural control of motor units. *Nature Neuroscience*, *25*(11), 1492–1504. https://doi.org/10.1038/s41593-022-01165-8

Martínez-Silva, M. de L., Imhoff-Manuel, R. D., Sharma, A., Heckman, C. J., Shneider, N. A., Roselli, F., Zytnicki, D., & Manuel, M. (2018). Hypoexcitability precedes denervation in the large fast-contracting motor units in two unrelated mouse models of ALS. *eLife*, *7*(2007), 1–26. https://doi.org/10.7554/eLife.30955

Mathewson, M. A., Chapman, M. A., Hentzen, E. R., Fridén, J., & Lieber, R. L. (2012). Anatomical, architectural, and biochemical diversity of the murine forelimb muscles. *Journal of Anatomy*, *221*(5), 443–451. https://doi.org/10.1111/j.1469-7580.2012.01559.x

Mathis, A., Mamidanna, P., Cury, K. M., Abe, T., Murthy, V. N., Mathis, M. W., & Bethge, M. (2018). DeepLabCut: Markerless pose estimation of user-defined body parts with deep learning. *Nature Neuroscience*, *21*(9), 1281–1289. https://doi.org/10.1038/s41593-018-0209-y

Mayer, W. P., & Akay, T. (2018). Stumbling corrective reaction elicited by mechanical and electrical stimulation of the saphenous nerve in walking mice. *Journal of Experimental Biology*, *221*(13). https://doi.org/10.1242/jeb.178095

Meehan, C. F., Sukiasyan, N., Zhang, M., Nielsen, J. B., & Hultborn, H. (2010). Intrinsic Properties of Mouse Lumbar Motoneurons Revealed by Intracellular Recording In Vivo. *Journal of Neurophysiology*, *103*(5), 2599–2610. https://doi.org/10.1152/jn.00668.2009

Mendes, C. S., Bartos, I., Márka, Z., Akay, T., Márka, S., & Mann, R. S. (2015). Quantification of gait parameters in freely walking rodents. *BMC Biology*, *13*(1), 1–11. https://doi.org/10.1186/s12915-015-0154-0

Menelaou, E., & McLean, D. L. (2012). A Gradient in Endogenous Rhythmicity and Oscillatory Drive Matches Recruitment Order in an Axial Motor Pool. *The Journal of Neuroscience*, *32*(32), 10925–10939. https://doi.org/10.1523/JNEUROSCI.1809-12.2012

Pachitariu, M., Steinmetz, N., Kadir, S., Carandini, M., & Kenneth D., H. (2016). Kilosort: Realtime spike-sorting for extracellular electrophysiology with hundreds of channels. *bioRxiv*, 061481. https://doi.org/10.1101/061481

Ritter, L. K., Tresch, M. C., Heckman, C. J., Manuel, M., & Tysseling, V. M. (2014). *Characterization of motor units in behaving adult mice shows a wide primary range*. 543–551. https://doi.org/10.1152/jn.00108.2014

Ryan, M. M., & Gregor, R. J. (1992). EMG profiles of lower extremity muscles during cycling at constant workload and cadence. *Journal of Electromyography and Kinesiology*, *2*(2), 69–80. https://doi.org/10.1016/1050-6411(92)90018-E

Sarver, J. J., Dishowitz, M. I., Kim, S.-Y., & Soslowsky, L. J. (2010). Transient decreases in forelimb gait and ground reaction forces following rotator cuff injury and repair in a rat model. *Journal of Biomechanics*, *43*(4), 778–782. https://doi.org/10.1016/j.jbiomech.2009.10.031

Schiaffino, S., & Reggiani, C. (2011). Fiber Types in Mammalian Skeletal Muscles. *Physiological Reviews*, *91*(4), 1447–1531. https://doi.org/10.1152/physrev.00031.2010

Schmitt, D., Zumwalt, A. C., & Hamrick, M. W. (2010). The relationship between bone mechanical properties and ground reaction forces in normal and hypermuscular mice. *Journal of Experimental Zoology Part A: Ecological Genetics and Physiology*, *313A*(6), 339–351. https://doi.org/10.1002/jez.604

Scholle, H. Ch., Schumann, N. P., Biedermann, F., Stegeman, D. F., Graßme, R., Roeleveld, K., Schilling, N., & Fischer, M. S. (2001). Spatiotemporal surface EMG characteristics from rat triceps brachii muscle during treadmill locomotion indicate selective recruitment of functionally distinct muscle regions. *Experimental Brain Research*, *138*(1), 26–36. https://doi.org/10.1007/s002210100685

Schumann, N. (2002). Multi-channel EMG of the M. triceps brachii in rats during treadmill locomotion. *Clinical Neurophysiology*, *113*(7), 1142–1151. https://doi.org/10.1016/S1388-2457(02)00143-8

Schumann, N. P., Biedermann, F. H. W., Arnold, D., Jinnah, H. A., Grassme, R., Fischer, M. S., & Scholle, H. C. (2006). Treadmill locomotion in normal mice—Step related multi-channel EMG profiles of thigh muscles. *Pathophysiology*, *13*(4), 245–255. https://doi.org/10.1016/j.pathophys.2006.09.002

Sober, S. J., Sponberg, S., Nemenman, I., & Ting, L. H. (2018). Millisecond Spike Timing Codes for Motor Control. *Trends in Neurosciences*, *41*(10), 644–648. https://doi.org/10.1016/j.tins.2018.08.010

Sponberg, S., Spence, A. J., Mullens, C. H., & Full, R. J. (2011). A single muscle's multifunctional control potential of body dynamics for postural control and running. *Philosophical Transactions of the Royal Society B: Biological Sciences*, *366*(1570), 1592–1605. https://doi.org/10.1098/rstb.2010.0367

Srivastava, K. H., Elemans, C. P. H., & Sober, S. J. (2015). Multifunctional and Context-Dependent Control of Vocal Acoustics by Individual Muscles. *The Journal of Neuroscience*, *35*(42), 14183–14194. https://doi.org/10.1523/JNEUROSCI.3610-14.2015

Srivastava, K. H., Holmes, C. M., Vellema, M., Pack, A. R., Elemans, C. P. H., Nemenman, I., & Sober, S. J. (2017). Motor control by precisely timed spike patterns. *Proceedings of the National Academy of Sciences of the United States of America*, *114*(5), 1171–1176. https://doi.org/10.1073/pnas.1611734114

Tata Ramalingasetty, S., Danner, S. M., Arreguit, J., Markin, S. N., Rodarie, D., Kathe, C., Courtine, G., Rybak, I. A., & Ijspeert, A. J. (2021). A Whole-Body Musculoskeletal Model of the Mouse. *IEEE Access*, *9*, 163861–163881. https://doi.org/10.1109/ACCESS.2021.3133078

Ting, L. H., & Chiel, H. J. (2017). Muscle, Biomechanics, and Implications for Neural Control. In

S. L. Hooper & A. Büschges (Eds.), *Neurobiology of Motor Control* (1st ed., pp. 365–416). Wiley. https://doi.org/10.1002/9781118873397.ch12

Van Ingen Schenau, G. J., Boots, P. J. M., De Groot, G., Snackers, R. J., & Van Woensel, W. W. L. M. (1992). The constrained control of force and position in multi-joint movements. *Neuroscience*, *46*(1), 197–207. https://doi.org/10.1016/0306-4522(92)90019-X

Van Ingen Schenau, G. J., Pratt, C. A., & Macpherson, J. M. (1994). Differential use and control of mono- and biarticular muscles. *Human Movement Science*, *13*(3–4), 495–517. https://doi.org/10.1016/0167-9457(94)90051-5

Watanabe, K., Vieira, T. M., Gallina, A., Kouzaki, M., & Moritani, T. (2021). Novel Insights Into Biarticular Muscle Actions Gained From High-Density Electromyogram. *Exercise and Sport Sciences Reviews*, *49*(3), 179–187. https://doi.org/10.1249/JES.0000000000000254

Zajac, F. E., & Young, J. L. (1980). Discharge properties of hindlimb motoneurons in decerebrate cats during locomotion induced by mesencephalic stimulation. *Journal of Neurophysiology*, *43*(5), 1221–1235. https://doi.org/10.1152/jn.1980.43.5.1221

Supplemental Figures

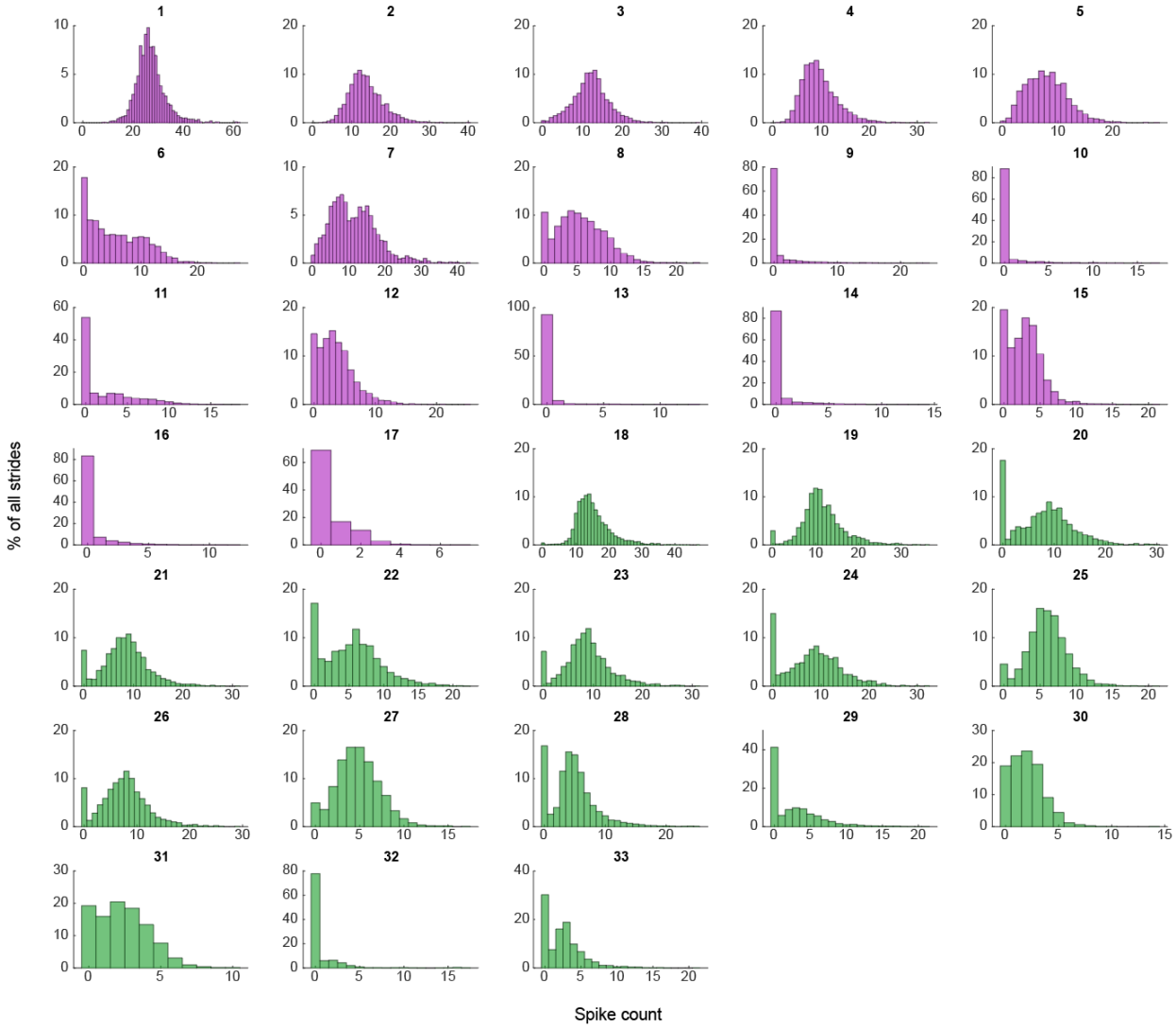

Supplemental Figure 1 - supplement to main text Figure 2. Empirical observations of spike count distributions for all units. Units are arranged sequentially to match the descending order presented in main text Figure 3.

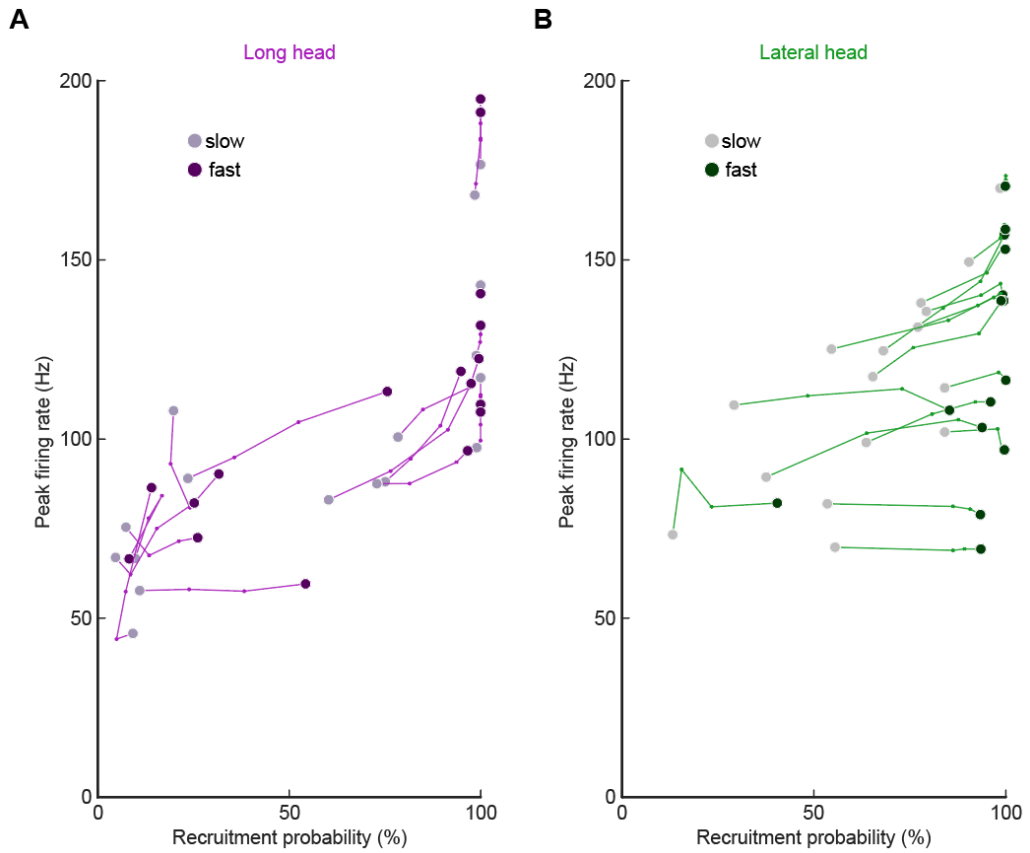

Supplemental Figure 2 - supplement to main text Figure 5: Altered firing rate and recruitment across walking speed quartiles for all motor units in the long head **(A)** and lateral head **(B)**. Each point reflects the median for the model estimate of each unit across the speeds.

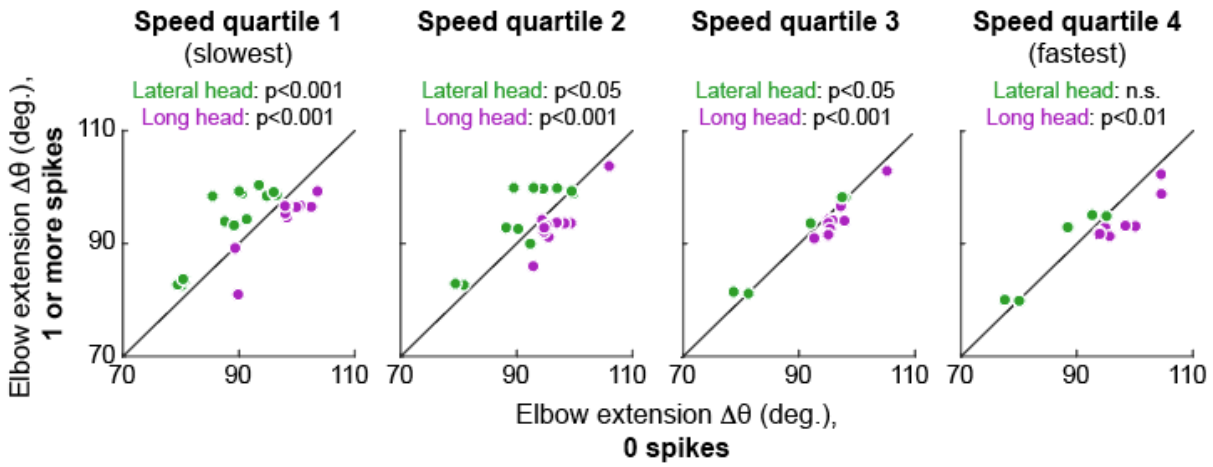

Supplemental Figure 3 - supplement to main text Figure 6: Plots show the same analysis as main text figure 6 for each individual speed quartile. Speed quartiles 1 and 4 are the slowest and fastest quartiles, respectively, and p-values refer to the results of Wilcoxon signed-rank tests performed separately on data from motor units of the lateral (green) and long (purple) heads of the triceps muscle.